Magnetizations and de Haas-van Alphen oscillations in massive Dirac fermions

F. R. Pratama [1,*] M. Shoufie Ukhtary [1,2] and Riichiro Saito [1]

[1]*Department of Physics, Tohoku University, Sendai 980-8578, Japan*

[2]*Research Center for Physics, Indonesian Institute of Sciences (LIPI), Tangerang Selatan 15314, Indonesia*

(Received 23 December 2020; revised 20 May 2021; accepted 20 May 2021; published 4 June 2021)

We theoretically study magnetic field, temperature, and energy band-gap dependences of magnetizations in the Dirac fermions. We use the zeta function regularization to obtain analytical expressions of thermodynamic potential, from which magnetization of graphene for strong field/low temperature and weak field/high temperature limits are calculated. Further, we generalize the result by considering the effects of impurity on orbital susceptibility of graphene. In particular, we show that in the presence of impurity, the susceptibility follows a scaling law which can be approximated by the Faddeeva function. In the case of massive Dirac fermions, we show that a large band gap gives a robust magnetization with respect to temperature and impurity. In the doped Dirac fermion, we discuss the dependences of period and amplitude of the de Haas-van Alphen oscillation on band gap.

DOI: 10.1103/PhysRevB.103.245408

I. INTRODUCTION

Historically, theoretical study on the magnetic properties of graphene [1–3] can be traced back to a paper by McClure [4] in 1956. He showed that diamagnetism in undoped graphene is largely contributed by coalescence of states of the massless Dirac electrons at the valence bands to the zeroth Landau levels (LLs) at the K and K' valleys in the hexagonal Brillouin zone in the presence of an external magnetic field. At the zeroth LLs, the free energy increases with increasing magnetic field, thus graphene shows orbital diamagnetism. Saito and Kamimura [5] showed that orbital paramagnetism appears in graphene intercalation compounds. Furthermore, Raoux *et al.* [6] demonstrated that the diamagnetism in a two-dimensional (2D) honeycomb lattice can be tuned into paramagnetism by introducing an additional hopping parameter, where the Berry phase is varying continuously between π and 0. The orbital paramagnetism in graphene can also occur as a result of many body interactions [7].

The analytical formula for orbital susceptibility of graphene can be derived by using the Kubo formula, as shown by Principi *et al.* [8]. A method to derive analytical formula for orbital susceptibility of a massive Dirac system is developed by Koshino and Ando [9,10]. In their method, the Euler-Maclaurin expansion formula is applied to calculate thermodynamic potential in the presence of magnetic field. They showed that pseudospin paramagnetism is responsible for a singular orbital susceptibility inside band-gap region and disappears when chemical potential enters the valence or conduction bands [9–11]. The expansion formula was first used by Landau [12] to demonstrate orbital diamagnetism in metals. In the context of graphene-related materials, the Euler-Maclaurin expansion is employed to calculate orbital susceptibilities of transition-metal dichalcogenides (TMDs) [13] and the Weyl semimetals [14]. However, magnetization as a function of magnetic field B and temperature T cannot be obtained by using the Euler-Maclaurin expansion formula. It is because that the magnetization diverges due to an infinite number of the LLs formed in the valence bands that are included in the calculation of the thermodynamic potential, unless a cutoff of the LLs is introduced [15,16]. The calculated magnetization M as a function of B has the form $M \propto C_1 - C_2 B$ ($C_2 > 0$), where the constant C_1 becomes infinite with increasing the number of the LLs, while in the case of a conventional metal, only the LLs in the conduction bands are considered. Moreover, the Euler-Maclaurin expansion method is valid only when the spacing of the LLs is much smaller than the thermal energy $k_B T$, where k_B is the Boltzmann constant [12].

In the recent study by Li *et al.* [17], magnetization of undoped graphene is measured for a wide range of B and temperature T. In the strong B/low T limit, it is shown that the magnetization is proportional to the square root of the magnetic field and diminishes linearly with increasing temperature ($M \propto -\sqrt{B} + \text{constant} \times T$), while in the weak B/high T limit, it is observed that the magnetization is proportional to B and inversely proportional to T ($M \propto -B/T$). The experimental data and numerical calculations are fitted into a Langevin function, from which the properties of magnetization for the two limiting cases can be deduced [17].

To avoid the divergence in the magnetization, we derive analytical formulas for thermodynamic potentials of the Dirac systems by using the zeta function regularization. In the context of quantum field theory, this method was used by Cangemi and Dunne [18] to calculate the energy of relativistic fermions in magnetic field. In graphene-related topics, the zeta function regularization was employed by Ghosal *et al.* [19] to explain the anomalous orbital diamagnetism of graphene at $T = 0$ K and by Slizovskiy and Betouras [20] to show

*pratama@flex.phys.tohoku.ac.jp

 ©2021 American Physical Society

nonlinear magnetization of graphene in a strong B. In this paper, we derive analytical formula for the magnetization of graphene for both the strong B/low T and weak B/high T limits by the zeta function regularization, which reproduces the Langevin fitting to the experimental observation. Further, we discuss the effect of impurity on orbital susceptibility of graphene. We show that in the presence of impurity, the orbital susceptibility as a function of temperature follows a scaling law which is approximately given by the so-called Faddeeva function. The effects of energy band gap on magnetizations in undoped and doped Dirac systems are also discussed. In the undoped case, large band gaps in monolayer TMDs yield relatively small but robust magnetizations with respect to temperature and impurity. In the doped case, we show that the opening of the band gap is observed from the diminishing amplitude of the de Haas-van Alphen (dHvA) oscillation at $T = 0$ K. This phenomenon cannot be obtained by the Euler-Maclaurin expansion method [4].

The paper is organized as follows. In Sec. II, we present analytical methods for calculating the LLs, thermodynamic potential, and magnetization. In Sec. III, calculated results are discussed. In Sec. IV, conclusion is given.

II. CALCULATION METHODS

A. The Landau levels of massive Dirac fermions

As a starting point, we consider a massive Dirac system with a band gap of $\Delta > 0$. We employ a 2×2 Hamiltonian matrix which is suitable to describe the energy spectra of a gapped graphene and monolayer transition-metal dichalcogenides (TMDs). The latter is enabled by including a nonzero spin-orbit coupling (SOC) constant λ in the Hamiltonian [21]. The energy dispersions are approximated by a linear function of momentum $\mathbf{p} = (p_x, p_y)$, and the Zeeman term is neglected because we only consider the cases when the Zeeman splitting is much smaller than the Landau levels (LLs) separation. In the presence of an external magnetic field $\mathbf{B} = B\hat{\mathbf{z}}$, the momentum acquires an additional term by the Peierl substitution, i.e., $\mathbf{p} \to \mathbf{p} + e\mathbf{A}$. The vector potential $\mathbf{A}$ is related to $\mathbf{B}$ by $\mathbf{B} = \nabla \times \mathbf{A}$. By choosing the Landau gauge $\mathbf{A} = (0, Bx)$, the Hamiltonian is given by [2,3,22]:

$$\hat{H}_{\tau s} = \begin{bmatrix} \Delta/2 & v_F\{\tau p_x - i(p_y + eBx)\} \\ v_F\{\tau p_x + i(p_y + eBx)\} & -\Delta/2 + \lambda\tau s \end{bmatrix}. \tag{1}$$

Here, v_F is the Fermi velocity whose typical value for the Dirac fermions is $\sim 10^6$ m/s, $\tau = +1\ (-1)$ is the index for the K (K') valley, and $s = +1\ (-1)$ is the index for spin-up (spin-down).

To solve Eq. (1), we define annihilation and creation operators $\hat{a} \equiv [\ell_B/(\sqrt{2}\hbar)][ip_x + (p_y + eBx)]$ and $\hat{a}^\dagger \equiv [\ell_B/(\sqrt{2}\hbar)][-ip_x + (p_y + eBx)]$, where $\ell_B = \sqrt{\hbar/(eB)}$ is the magnetic length. In term of the annihilation and creation operators, the Hamiltonian for a given τ and s reduces to

$$\hat{H}_\xi = \begin{bmatrix} \Delta/2 & -i\hbar\omega_c\hat{O}_\tau \\ i\hbar\omega_c\hat{O}_\tau^\dagger & -\Delta/2 + \lambda\xi \end{bmatrix}, \tag{2}$$

where $\xi \equiv \tau s$, $\hat{O}_+ \equiv \hat{a}$, $\hat{O}_- \equiv \hat{a}^\dagger$, and $\omega_c = \sqrt{2}v_F/\ell_B = \sqrt{2{v_F}^2 eB/\hbar}$ is the cyclotron frequency of the Dirac fermions. $\xi = +1(-1)$ represents the spin-up (spin-down) electron at the K valley or spin-down (spin-up) electron at K' valley. The nth LLs ϵ_n^ξ and wave function $|\Psi_n^\xi\rangle$ are given by the eigenvalues and eigenvectors of Eq. (2), respectively, as follows:

$$\epsilon_n^\xi = \frac{\xi\lambda}{2} + \mathrm{sgn}_\tau(n)\sqrt{(\hbar\omega_c)^2|n| + \left(\frac{\Delta_\xi}{2}\right)^2} \tag{3}$$

and

$$\left|\Psi_n^\xi\right\rangle = \frac{1}{\sqrt{2\left|\epsilon_n^\xi - \frac{\xi\lambda}{2}\right|}}\begin{bmatrix} -i\sqrt{|\epsilon_n^\xi + \frac{\Delta}{2} - \lambda\xi}||\alpha_n^\tau\rangle \\ \sqrt{|\epsilon_n^\xi - \frac{\Delta}{2}}||\beta_n^\tau\rangle \end{bmatrix}, \tag{4}$$

where we define $\Delta_\xi \equiv \Delta - \xi\lambda$ as a shorthand notation. It is noted that in the absence of the SOC ($\lambda = 0$), we drop the superscript ξ in Eqs. (3) and (4). $\mathrm{sgn}_\tau(n)$ is the sign function defined by $\mathrm{sgn}_\tau(n) = -1$ for $n < 0$ and $\mathrm{sgn}_\tau(n) = +1$ for $n > 0$. For $n = 0$, a nontrivial wave function is satisfied by choosing $\mathrm{sgn}_+(0) = -1$ and $\mathrm{sgn}_-(0) = +1$. $|\alpha_n^\tau\rangle$ and $|\beta_n^\tau\rangle$ are opposite for the K and K' valleys, i.e., $|\alpha_n^+\rangle = |\beta_n^-\rangle \equiv ||n| - 1\rangle$ and $|\alpha_n^-\rangle = |\beta_n^+\rangle \equiv ||n|\rangle$, where $||n|\rangle$ is a normalized states such that $\hat{a}||n|\rangle = \sqrt{|n|}||n| - 1\rangle$ and $\hat{a}^\dagger||n|\rangle = \sqrt{|n| + 1}||n| + 1\rangle$. The zeroth LLs at the K and K' valleys exist at the valence and the conduction bands, respectively [9,10]. The existence of only one zeroth LL in each valley is confirmed by first-principle calculations for hexagonal boron nitride (h-BN) and MoS_2 [23]. For $\Delta < 0$ and $\lambda = 0$, a nontrivial wave function for $n = 0$ is satisfied by $\mathrm{sgn}_+(0) = +1$ and $\mathrm{sgn}_-(0) = -1$, as in the case of topological silicene [24]. Nevertheless, in this study we only consider $\Delta > 0$ without losing generality because it will be shown that the magnetization of the Dirac system depends only on the absolute value of Δ, and not on the sign. It is noted that our convention of the K and K' valleys is same as used in references [9,10,25] which is opposite of those references [13,26].

In Fig. 1, we plot the LLs ($n = -5$ to $n = 5$) of a gapped graphene [(a) and (b)] and monolayer MoS_2 [(c)–(f)] at the K and the K' valleys as a function of the magnetic field B. In (a) and (b), the LLs of the gapped graphene with $\Delta = 100$ meV, $\lambda = 0$, and $v_F = 10^6$ m/s show $\sqrt{B}$ dependences, because $\Delta/2$ is smaller than the cyclotron energy $\hbar\omega_c$ (72.5 meV for $B = 4$ T). In Figs. 1(c)–1(f), the LLs of MoS_2 at the conduction bands [(c) and (d)] and the valence bands [(e) and (f)] are shown, where we adopt $\Delta = 1.66$ eV, $\lambda = 75$ meV, and $v_F = 5.3 \times 10^5$ m/s [21,25–27]. We can see that the SOC generates spin splitting between the spin-up (red-solid lines) and the spin-down (blue-dashed lines) electrons except for the zeroth LLs at the K' valley [Fig. 1(d)]. For the valence band, a spin splitting $2\lambda = 150$ meV occurs for the zeroth LLs at the K valley [Fig. 1(e)]. The LLs are linearly dependent for $B =$ 0–20 T because $\Delta/2$ is ten times larger than $\hbar\omega_c = 0.086$ eV for $B = 20$ T.

B. Thermodynamic potential and magnetization

By assuming an electron-doped system, the total thermodynamic potential per unit area in the presence of magnetic

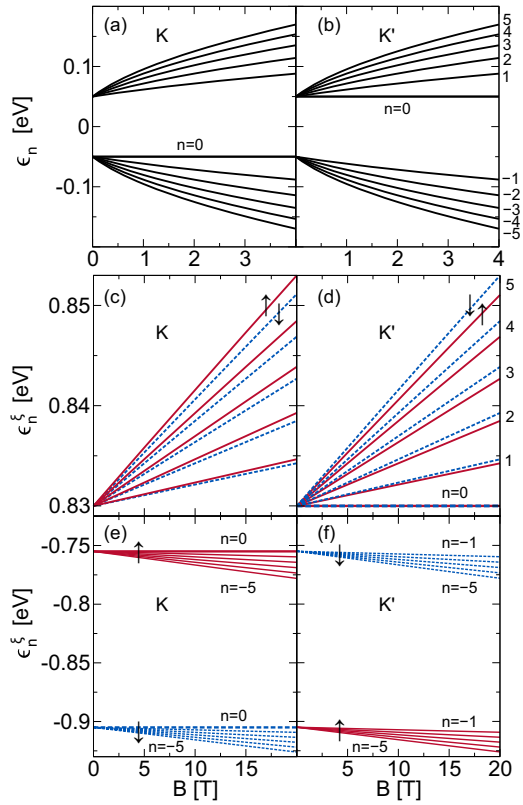

FIG. 1. The LLs ($n = -5$ to $n = 5$) of the massive Dirac systems. The figures on the left (right) side correspond to the LLs at the K (K') valley. (a),(b): the LLs of a gapped graphene ($\Delta = 100$ meV, $\lambda = 0$, and $v_F = 10^6$ m/s) for $B = 0$–4 T. (c)–(f) The LLs of MoS_2 ($\Delta = 1.66$ eV, $\lambda = 75$ meV, and $v_F = 5.3 \times 10^5$ m/s) for $B = 0$–20 T. The LLs for the spin-up and spin-down electrons are shown with red-solid and blue-dashed lines, respectively.

field is given by

$$\Omega = -\frac{1}{\beta}\frac{eB}{h}\sum_{\xi=\pm}\sum_{n=-\infty}^{\nu_\xi}\ln[1+e^{-\beta(\epsilon_n^\xi-\mu)}]$$
$$\equiv [\Omega_- + \Omega_+^{(e)}], \tag{5}$$

where $\beta = 1/(k_B T)$ and μ is chemical potential. The prefactor eB/h represents the Landau degeneracy per unit area. The summation in Eq. (5) is carried out up to ν_ξ, which is defined as the index of the highest occupied LLs at the conduction bands, that is obtained from Eq. (3) by setting $\mu = \epsilon_\nu^\xi$ and solving for n as follows:

$$\nu_\xi \equiv \left\lfloor \frac{(\mu - \xi\lambda/2)^2 - (\Delta_\xi/2)^2}{(\hbar\omega_c)^2} \right\rfloor \equiv \lfloor \tilde{\nu}_\xi \rfloor, \tag{6}$$

where the floor function $\lfloor x \rfloor$ is gives by the greatest integer smaller than or equal to x. It is noted that for $\lambda = 0$, we drop the summation of ξ in Eq. (5) and multiply the thermodynamic potentials by $g_s = 2$ to account the spin degeneracy. Similarly, we drop the subscript ξ in Eq. (6). For expository purposes, we define Ω_- and $\Omega_+^{(e)}$ as thermodynamic potentials for the occupied LLs at the valence and conduction bands, respectively, as illustrated in Fig. 2. We also define potential

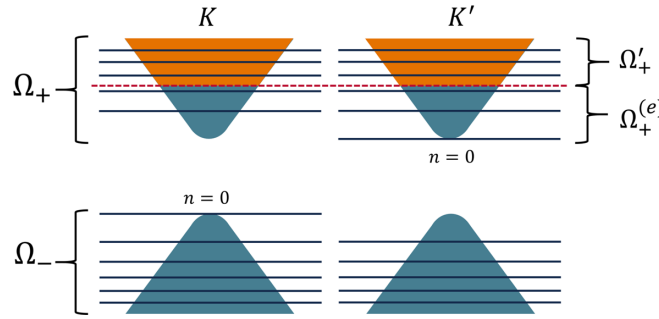

FIG. 2. Schematic definitions of Ω_-, Ω_+, $\Omega_+^{(e)}$, and Ω'_+ for electron-doped gapped graphene. The black and red lines represent the LLs and the level of chemical potential μ, respectively.

which includes all the LLs at the conduction bands, Ω_+, as well as potential for $n = \nu_\xi + 1$ to $n = \infty$ LLs, Ω'_+. Thus, we have the relation $\Omega_+^{(e)} = \Omega_+ - \Omega'_+$. It shall be shown that Ω'_+ and Ω_+ are relevant for the calculations at high temperature. After obtaining an analytical expression of Ω, magnetization is calculated by

$$M(B, \mu, T) = -\frac{\partial\Omega(B, \mu, T)}{\partial B}. \tag{7}$$

In the presence of impurity, magnetization for a given scattering rate γ is calculated by convolution of M in Eq. (7) with a Lorentzian profile as follows [28–32]:

$$M(\mu, T, \gamma) = \frac{\gamma}{\pi}\int_{-\infty}^{\infty} d\varepsilon M(\varepsilon, T)\frac{1}{(\varepsilon-\mu)^2+\gamma^2}. \tag{8}$$

The parameter γ is related to the self-energy due to impurity scattering, and γ is inversely proportional to the relaxation time of the quasiparticle. For simplicity, we assume that γ is independent of B and T, and therefore the susceptibility as a function of temperature is given by $\chi(\mu, T, \gamma) = [\partial M(\mu, T, \gamma)/\partial B]_{B=0}$. In the following discussions, we consider two cases: (1) low temperature ($T \to 0$ K or $\hbar\omega_c \gg k_B T$) and (2) high temperature ($\hbar\omega_c \ll k_B T$).

III. RESULTS

In this study, we consider several cases of magnetization depending on (1) either gapless ($\Delta = 0$) or gapped ($\Delta \neq 0$), (2) either undoped ($\mu = 0$) or doped ($\mu \neq 0$), (3) either without ($\lambda = 0$) or with SOC ($\lambda \neq 0$). In Table I, we summarize the results of M and the dHvA effect for quick understanding. It is noted that we do not consider the two cases, $\Delta = 0$, $\mu = 0$ or $\mu \neq 0$, and $\lambda \neq 0$.

A. Thermodynamic potential of massive Dirac fermion ($T = 0$ K, any Δ, λ, and μ)

First, let us derive thermodynamic potentials for $T = 0$ K. Since we consider the electron-doped system, we set $\mu \geqslant \Delta/2$. The logarithmic function in Eq. (5) is approximated by $\ln[1 + \exp\{-\beta(\epsilon_n^\xi - \mu)\}] \approx -\beta(\epsilon_n^\xi - \mu)$ which is valid in the case of $-(\epsilon_n^\xi - \mu) \gg k_B T$ or $T \to 0$ K. The thermodynamic potential for the occupied LLs with $n \leqslant 0$, Ω_- is

TABLE I. Summary of magnetization behaviours of the Dirac fermions for a given T, Δ, λ, and μ. *) The derivations of M are not explicitly given, in which we only give the expressions of Ω.

System	Δ	λ	μ	Magnetization	Eq. No.	Fig. No.
Graphene	0	0	0	$M = -\frac{0.882e^{3/2}v_F}{\pi\hbar^{1/2}}\sqrt{B} + \frac{2\ln(2)ek_B}{\pi\hbar}T$ $[\hbar\omega_c \gg k_BT]$	Eq. (20)	Fig. 3
				$M = -\frac{(ev_F)^2}{6\pi k_BT}B + \mathcal{O}(B^3)$ $[\hbar\omega_c \ll k_BT]$		Fig. 4
	0	0	$\neq 0$	dHvA effect is observed $[T = 0\ \mathrm{K}]$	Eq. (25)	Fig 6
				$M = \frac{4g_s}{\beta}\frac{e}{h}\sum_{\ell=1}^{\infty}\mathrm{Li}_{1-2\ell}(-e^{\beta\mu})\frac{(2\hbar{v_F}^2e\beta^2B)^\ell}{(2\ell)!}\mathcal{B}_{\ell+1}$ $[\hbar\omega_c \ll k_BT]$	Eq. (18)	-
Gapped graphene	$\neq 0$	0	0	$M \propto -\sqrt{B}$ $[T = 0\ \mathrm{K},\ \hbar\omega_c \gg \Delta]*$	Eq. (9)	Fig. 5
				$M \propto -\frac{B}{\Delta}$ $[T = 0\ \mathrm{K},\ \hbar\omega_c \ll \Delta]*$		
				$M \approx -\frac{(ev_F)^2}{6\pi k_BT}B$ $[\hbar\omega_c \sim \Delta \ll k_BT]*$	Eq. (13)	-
	$\neq 0$	0	$\neq 0$	dHvA effect is observed $[T = 0\ \mathrm{K}]$	Eq. (25)	Fig 6
				$M \approx -\frac{(ev_F)^2B}{6\pi k_BT}\mathrm{sech}^2(\frac{\mu}{2k_BT})$ $[\hbar\omega_c \sim \Delta \ll k_BT]*$	Eq. (13)	-
TMDs	$\neq 0$	$\neq 0$	0	$M \approx -\frac{(ev_F)^2B}{3\pi}\sum_{\xi=\pm1}\frac{1}{\Delta_\xi}$ $[T = 0\ \mathrm{K}]*$	Eq. (A4)	-
				$M \approx -\frac{(ev_F)^2B}{3\pi}\sum_{\xi=\pm1}\frac{1}{\Delta_\xi}\tanh[\frac{\beta\Delta_\xi}{2}]$ $[\hbar\omega_c \sim k_BT]*$	Eq. (26)	Fig. 7
	$\neq 0$	$\neq 0$	$\neq 0$	$M \approx -\frac{(ev_F)^2B}{3\pi}\sum_{\xi=\pm}\frac{1}{\Delta_\xi}\frac{\sinh[\frac{\beta\Delta_\xi}{2}]}{\cosh[\frac{\beta\Delta_\xi}{2}]+\cosh[\beta(\mu-\frac{\xi\lambda}{2})]}$ $[\hbar\omega_c \sim k_BT]*$	Eq. (26)	Fig. 7

expressed by (see Appendix A 1 for derivation)

$$\Omega_- = -2\frac{eB}{h}\sum_{\xi=\pm}\left[\hbar\omega_c\zeta\Big(-\frac{1}{2},{\Gamma_\xi}^2\Big) - \frac{\Delta_\xi}{4}\right], \tag{9}$$

where we define $\Gamma_\xi \equiv \Delta_\xi/(2\hbar\omega_c)$, and the infinite summation of the LLs is given by the Hurwitz zeta function, which is defined by (see for example Ref. [33])

$$\zeta(p,q) \equiv \sum_{k=0}^{\infty}\frac{1}{(k+q)^p}. \tag{10}$$

It is noted that the chemical potential μ does not appear in the expression of Ω_- for the electron-doped system. Equation (9) gives intrinsic diamagnetism of the Dirac fermions. A similar result was derived by Sharapov *et al.* [28] for a gapped graphene, which is obtained by introducing an ultraviolet cut-off in the calculation of the thermodynamic potential.

In the calculation of $\Omega_+^{(e)}$, we introduce the step function $\Theta(\mu - \Delta/2)$ as a threshold to make sure that $\Omega_+^{(e)}$ is relevant when the doping level is larger than the band gap, as follows (see Appendix A 2 for derivation):

$$\Omega_+^{(e)} = -2\frac{eB}{h}\sum_{\xi=\pm}\left[\frac{\Delta}{4} + \mu\Big(\nu_\xi + \frac{1}{2}\Big) - \frac{\xi\lambda}{2}(\nu_\xi + 1) + \hbar\omega_c\left\{\zeta\Big(-\frac{1}{2},{\Gamma_\xi}^2 + \nu_\xi + 1\Big) - \zeta\Big(-\frac{1}{2},{\Gamma_\xi}^2\Big)\right\}\right] \times \Theta(\mu - \Delta/2). \tag{11}$$

In the derivation of Eq. (11), we need the fact that the finite summation of the LLs is expressed by a subtraction of two zeta functions as follows [33]:

$$\sum_{n=0}^{N}(n+q)^{-p} = \zeta(p,q) - \zeta(p,q+N+1). \tag{12}$$

In Appendix B, we show that the numerical calculation of the left-hand side of Eq. (12) reproduces the analytical expression on the right-hand side. Therefore, for massive Dirac fermions at $T = 0$ K, the total thermodynamic potential [Eq. (5)] is obtained by substituting the results in Eqs. (9) and (11) for Ω_- and $\Omega_+^{(e)}$, respectively.

B. Thermodynamic potential of massive Dirac fermion $[k_BT \gg (\hbar\omega_c \sim \Delta), \lambda = 0, \text{any } \mu]$

Now, let us derive thermodynamic potentials of a gapped graphene at high temperature. Here, we express $\Omega_+^{(e)} = \Omega_+ - \Omega'_+$ (see Fig. 2) when applying Eq. (5). In Appendix A 3, we show that Ω'_+ is negligible for $\hbar\omega_c \ll \mu \ll k_BT$, which indicates that electrons can occupy an indefinite number of the LLs at the conduction bands by thermal excitation. We expand the logarithmic and exponential terms in the first line of Eq. (5) which is valid for $[-\epsilon_n + \mu] \ll k_BT$. Ω is given by a power series of $(\hbar\omega_c)^2$ as follows (see Appendix A 3 for the derivation):

$$\Omega = \frac{4g_s}{\beta}\frac{eB}{h}\sum_{\ell=0}^{\infty}\mathrm{Li}_{1-2\ell}(-e^{\beta\mu})\frac{(\beta\hbar\omega_c)^{2\ell}}{(2\ell)!}\left[\zeta(-\ell,\Gamma^2) - \frac{\Gamma^{2\ell}}{2}\right] \equiv \sum_{\ell=0}^{\infty}\Omega_\ell. \tag{13}$$

It is noted that the dependence of Ω on μ is given by the polylogarithm function $\mathrm{Li}_s(z) \equiv \sum_{k=1}^{\infty} z^k/k^s$, which converges for $|z| \geqslant 1$ through analytical continuation [33].

C. Magnetization of graphene ($k_BT \gg \hbar\omega_c$ or $k_BT \ll \hbar\omega_c$, $\Delta = 0$, $\lambda = 0$, and any μ)

The LL of graphene is given by $\epsilon_n = \mathrm{sgn}_\tau(n)\hbar\omega_c\sqrt{n}$. $\epsilon_0 = 0$ is shared between the valence and conduction bands at the K and K' valleys, respectively. At $T = 0$ K and $\mu = 0$, ϵ_0 is half occupied [17]. By separating the zeroth LLs from the $n \neq 0$ LLs, Ω_- and $\Omega_+^{(e)}$ for $\hbar\omega_c \gg k_BT$ are given by

$$\begin{aligned}\Omega_- &= -\frac{g_s}{\beta}\frac{eB}{h}\left[\ln\{1+e^{\beta\mu}\} + 2\sum_{n=1}^{\infty}\ln\{1+e^{\beta(\hbar\omega_c\sqrt{n}+\mu)}\}\right] \\ &= -2g_s\frac{eB}{h}\left[\frac{1}{2\beta}\ln\{1+e^{\beta\mu}\} + \hbar\omega_c\zeta\Big(-\frac{1}{2},1\Big) - \frac{\mu}{2}\right],\end{aligned} \tag{14}$$

and

$$\begin{aligned}\Omega_+^{(e)} &= -\frac{g_s}{\beta}\frac{eB}{h}\left[\ln\{1+e^{\beta\mu}\} + 2\sum_{n=1}^{\nu}\ln\{1+e^{-\beta(\hbar\omega_c\sqrt{n}-\mu)}\}\right] \\ &= -2g_s\frac{eB}{h}\left[\frac{1}{2\beta}\ln\{1+e^{\beta\mu}\} + \mu\nu \right. \\ &\quad \left. + \hbar\omega_c\left\{\zeta\Big(-\frac{1}{2},1+\nu\Big) - \zeta\Big(-\frac{1}{2},1\Big)\right\}\right],\end{aligned} \tag{15}$$

respectively. We can confirm that by putting $T \to 0$ K, Eqs. (9) and (11) reduce to Eqs. (14) and (15) in the case of $\Delta = \lambda = 0$. In undoped graphene ($\mu = 0$), only the first term in the right-hand side of Eq. (15) survives and therefore Ω is given by

$$\begin{aligned}\Omega(\mu = 0) &= -2g_s\frac{eB}{h}\left[\hbar\omega_c\zeta\Big(-\frac{1}{2},1\Big) + \frac{1}{\beta}\ln(2)\right] \\ &\equiv \Omega_B + \Omega_S.\end{aligned} \tag{16}$$

Since the thermodynamic potential at $\mu = 0$ can be equivalently expressed by $\Omega = E - TS$, where E is internal energy and S is entropy, we identify that Ω_B and Ω_S in Eq. (16) are potentials associated with E from the $n < 0$ LLs and S of the $n = 0$ LLs, respectively. The origin of the $\ln(2)$ factor in the expression of Ω_S is two freedoms per valley, spin, and the LL degeneracies of the zeroth LLs. General formula for the entropy is given by $S = (\text{degeneracies}) \times k_B \ln W$, where W is the number of freedoms for occupying one electron. Because the energy of the zeroth LLs at the K and K' valleys consist of valence (K) and conduction (K') bands, the electron acquires two possible freedoms, i.e., for occupying the zeroth LL from the valence band while that of the conduction band is empty, and vice versa ($W = 2$). It is noted that we cannot distinguish the two freedoms. This argument also explains that $n < 0$ LLs do not contribute to the entropy because they are fully occupied ($W = 1$).

In the case of $\hbar\omega_c \ll k_BT$, Ω is obtained from Eq. (13) by putting $\Gamma = 0$, as follows:

$$\Omega = \frac{-4g_s}{\beta}\frac{eB}{h}\sum_{\ell=1}^{\infty}\mathrm{Li}_{1-2\ell}(-e^{\beta\mu})\frac{(\beta\hbar\omega_c)^{2\ell}}{(2\ell)!}\frac{\mathcal{B}_{\ell+1}}{\ell+1}, \tag{17}$$

where the Bernoulli number $\mathcal{B}_{\ell+1}$ is related to the zeta function by $\zeta(-\ell,0) = -\mathcal{B}_{\ell+1}/(\ell+1)$. The summation of ℓ in Eq. (17) begins from $\ell = 1$, because the term for $\ell = 0$ in Eq. (13) is independent of B and proportional to Δ^2, therefore for graphene $\Omega_0 = 0$ (see Appendix A 3). The magnetization of graphene for a given μ is given by

$$M = \frac{4g_s}{\beta}\frac{e}{h}\sum_{\ell=1}^{\infty}\mathrm{Li}_{1-2\ell}(-e^{\beta\mu})\frac{(2\hbar{v_F}^2e\beta^2B)^{\ell}}{(2\ell)!}\mathcal{B}_{\ell+1}. \tag{18}$$

Since $\mathrm{Li}_{-1}(z) = z/(1-z)^2$, we reproduce the formula for susceptibility of graphene derived by McClure [4] by considering a cutoff of the LLs at the conduction bands:

$$\chi = -\frac{e^2{v_F}^2}{6\pi k_BT}\mathrm{sech}^2\Big(\frac{\mu}{2k_BT}\Big). \tag{19}$$

It is noted that Eq. (19) is valid for any temperature $T > 0$ K because we take $B = 0$ to calculate χ, thus the condition $\hbar\omega_c \ll k_BT$ is always satisfied.

From Eqs. (16) and (18), magnetization of undoped graphene ($\mu = 0$) is given by

$$M = \begin{cases} -\dfrac{0.882}{\pi}\dfrac{e^{3/2}v_F}{\hbar^{1/2}}\sqrt{B} + \dfrac{2\ln(2)}{\pi}\dfrac{e}{\hbar}k_BT, & (\hbar\omega_c \gg k_BT), \\ -\dfrac{1}{6}\dfrac{e^2{v_F}^2}{\pi}\dfrac{B}{k_BT} + \mathcal{O}(B^3), & (\hbar\omega_c \ll k_BT). \end{cases} \tag{20}$$

Here, in Eq. (20) for $\hbar\omega_c \ll k_BT$, only odd powers of B survive because the Bernoulli number of $\mathcal{B}_{\ell+1}$ is zero for even $\ell > 0$.

The analytical expressions given by Eq. (20) can be directly compared with the work of Li *et al.* [17]. In their study, numerical calculation and experimental measurement of the magnetization for undoped graphene as a function of B and T are fitted into a Langevin function $L(x) = \coth(x) - 1/x$ as follows:

$$M = -\frac{0.882}{\pi}\frac{e^{3/2}v_F\sqrt{B}}{\hbar^{1/2}}L\left(\frac{\sqrt{\hbar v_F^2 eB\alpha(T)}}{\sqrt{2}k_BT}\right). \tag{21}$$

The temperature dependence of M is approximated by the function $\alpha(T) \equiv C/(C + \sqrt{T})$, where $C = 45\ \mathrm{K}^{1/2}$. Since $L(x) \sim x/3$ as $x \to 0$ and $L(x)$ is saturated to 1 as $x \to \infty$, the magnetization is given by [17]:

$$M \approx \begin{cases} -\dfrac{0.882}{\pi}\dfrac{e^{3/2}v_F}{\hbar^{1/2}}\sqrt{B} + \dfrac{0.882\sqrt{2}}{\pi}\dfrac{e}{\hbar}k_BT, & (\hbar\omega_c \gg k_BT), \\ -\dfrac{0.882}{3\sqrt{2}}\dfrac{e^2{v_F}^2}{\pi}\dfrac{B}{k_BT}, & (\hbar\omega_c \ll k_BT). \end{cases} \tag{22}$$

By comparing Eq. (20) with Eq. (22), the analytical formula reproduces experimentally observed B and T dependences

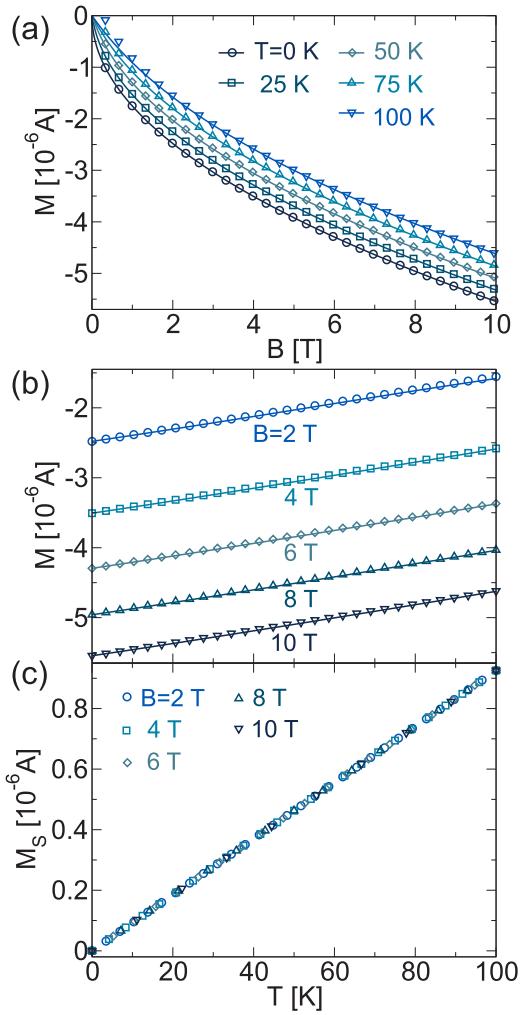

FIG. 3. Magnetization of graphene at $\hbar\omega_c \gg k_BT$ limit as a function of magnetic field and temperature. (a) M as a function of $B = 0$–10 T at fixed temperatures, (b) M, and (c) M_S as a function of T ($T = 0$–100 K) for several values of B. The calculations from analytical formula [Eq. (20)] and the Langevin function [Eq. (21)] are depicted by symbols and lines, respectively.

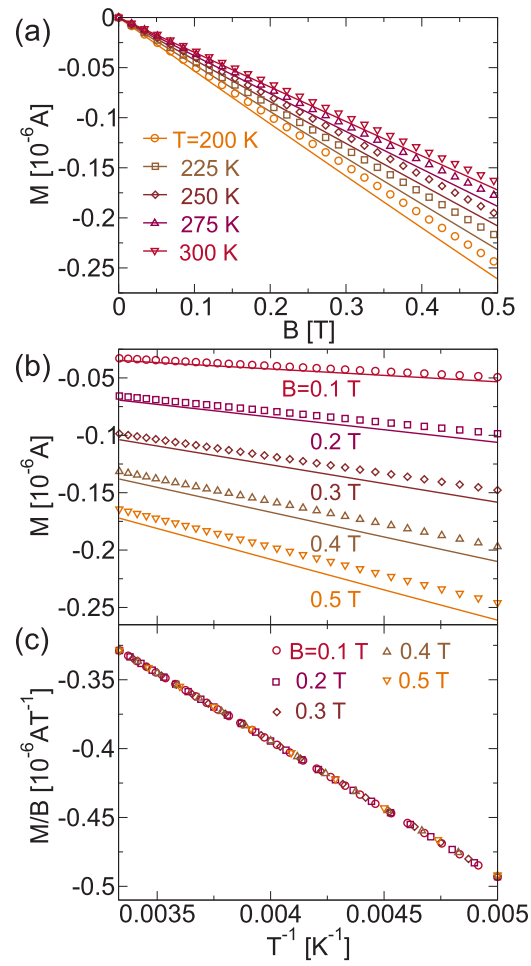

FIG. 4. Magnetization of graphene at $\hbar\omega_c \ll k_BT$ limit as a function of magnetic field and temperature. (a) M as a function of $B = 0$–0.5 T at fixed temperatures, (b) M, and (c) M/B as a function $1/T$ ($T = 200$–300 K) for several values of B. The calculations from analytical formula [Eq. (20)] and the Langevin function [Eq. (21)] are depicted by symbols and lines, respectively.

of the magnetization of graphene both for $\hbar\omega_c \gg k_BT$ and $\hbar\omega_c \ll k_BT$. It suggest that the zeta function regularization works reasonably.

In Fig. 3(a), we plot $M(B, T)$ for $\hbar\omega_c \gg k_BT$ as a function of B for several values of T by the analytical expression Eq. (20) (symbols) and the Langevin function Eq. (21) (lines). We can see that Eq. (20) works well at temperature as high as $T = 100$ K for $B \geqslant 1$ T, but for $B < 1$ T, Eq. (20) overestimates the temperature dependence of the magnetization because the condition $\hbar\omega_c \gg k_BT$ is not satisfied. In Fig. 3(b) we show M as a function of T for several values of B. The linear dependence of M on T at strong magnetic field originates from the entropy S of electrons which coalesce to the zeroth LLs [see Eq. (16)]. In Fig. 3(c), we plot $M_S \equiv M + C\sqrt{B}$, with $C \equiv 0.882e^{3/2}v_F/(\pi\hbar^{1/2})$ [see Eq. (20)] as a function of T for several values of B. M_S is a deviation from the intrinsic diamagnetism as temperature increases and does not depend on B. Interestingly, the gradient of M_S on T in Fig. 3(c) is given by fundamental constants $[2\ln(2)/\pi]ek_B/\hbar = 9.256 \times 10^{-9}$ A/K.

In Fig. 4(a), we plot $M(B, T)$ for $\hbar\omega_c \ll k_BT$ as a function of B for several values of T by the analytical expression Eq. (20) (symbols) and the Langevin function Eq. (21) (lines), where the linear B dependences of M for $B \leqslant 0.5$ T are observed at temperature as low as $T = 200$ K, especially for weak $B \sim 0.1$ T. For stronger B, Eqs. (20) and (21) begin to show some discrepancies. In Fig. 4(b), M is plotted as a function of $1/T$ for several values of B. In Fig. 4(c), the function M/B is plotted as a function of $1/T$ and is aligned into a straight line which illustrates $M \propto -B/T$ dependence. Here, the linear T^{-1} dependence of M at weak magnetic field originates from the thermal excitation of electron from valence to conduction bands, because in the derivation of Eq. (13), we include the entire LLs at both bands.

Magnetization of a doped graphene at $\hbar\omega_c \ll k_BT$ rapidly decreases with increasing μ, because of the leading factor, $\mathrm{Li}_{-1}(-e^{\beta\mu}) = \mathrm{sech}^2[\mu/(2k_BT)]/4$ in Eq. (18). On the other hand, magnetization of doped graphene at $T = 0$ K shows

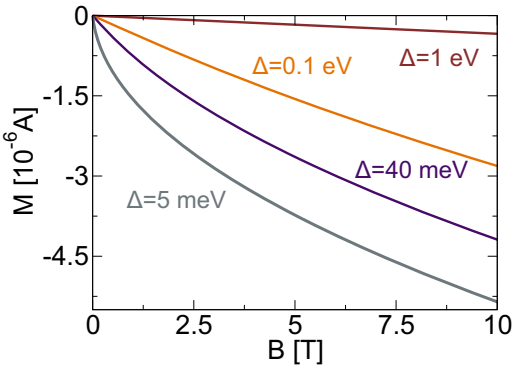

FIG. 5. Magnetization of massive Dirac fermions ($\Delta = 5$ meV, 40 meV, 0.1 eV, and 1 eV) as a function $B = 0$–10 T at $T = 0$ K. The value of chemical potential is $\mu = 0$ meV.

the dHvA effect, which will be discussed in the next section together with the case of gapped graphene, in order to uncover the effect of band gap on the period and amplitude of the dHvA oscillation. The explicit magnetization for both graphene ($\Delta = 0$) and gapped graphene ($\Delta \neq 0$) is given by Eq. (25) in Sec. III D.

D. Magnetization and dHvA effect of graphene and gapped graphene ($T = 0$ K, any Δ, $\lambda = 0$, any μ)

In Fig. 5, we plot magnetization of undoped ($\mu = 0$), massive Dirac fermions as a function of B for several values of Δ at $T = 0$ K. We can see that the magnetization undergoes a gradual change from $M \propto -\sqrt{B}$ to $M \propto -B$ dependences with increasing Δ for $B = 1$–10 T, which indicates that the anomalous orbital diamagnetism for $\Delta = 0$ disappears with the opening of the band gap. In this case, the spacing of the LLs which is initially $\sqrt{|n|}$ dependence becomes constant $(\hbar\omega_c)^2/\Delta$ with increasing Δ. This process can be observed by the transition from the topological to the trivial phases of undoped silicene, in which the band gap can be controlled by applying an external electric field [34] perpendicular to the silicene plane. A similar transition is predicted in graphene with increasing temperature for the same reason, in which the $\sqrt{|n|}$ dependence of the LLs in the valence bands is responsible for the $M \propto -\sqrt{B}$ dependence. When the thermal energy becomes larger than the cyclotron energy, the effect of $\sqrt{|n|}$ spacing of the LLs on the magnetization becomes no more important, and thus the Dirac system shows linear response $M \propto -B$ at a high T.

The oscillation of magnetization in a uniform magnetic field, which is known as the de Haas-van Alphen (dHvA) effect, has been observed experimentally in a quasi-2D system of graphite [35]. Much of the theoretical studies on the magnetic oscillations in the 2D systems [36–40] have been carried out within the framework of a generalized Lifshits-Kosevich (LK) [41] theory, which was proposed to account for magnetic oscillations in metals. In the LK theory, the dHvA effect is expressed by adding an oscillatory term to the Euler-Maclaurin formula (also known as the Poisson summation formula) for calculating the thermodynamic potential [41].

By assuming a fixed $\mu > \Delta/2$ and $\lambda = 0$ in Eqs. (9) and (11), let us discuss the effect of band gap on the period and

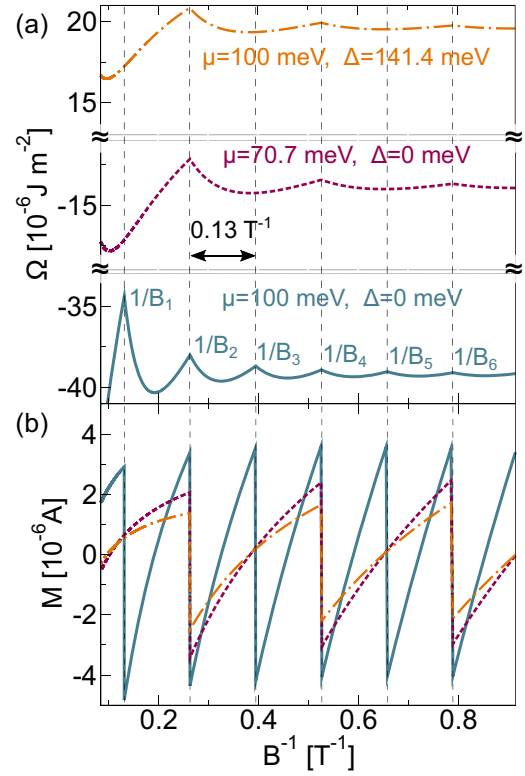

FIG. 6. Oscillations of (a) thermodynamic potential and (b) magnetization for $\mu = 100$ meV, $\Delta = 0$ meV (solid lines), $\mu = 70.7$ meV, $\Delta = 0$ meV (dashed lines), and $\mu = 100$ meV, $\Delta = 141.4$ meV (dash-dotted lines) at $T = 0$ K.

amplitude of the dHvA oscillation at $T = 0$ K. In the bottom panel of Fig. 6(a), we plot Ω for $\mu = 100$ meV and $\Delta = 0$ meV as a function of inverse magnetic field $1/B$. At several values of $1/B$ (labeled as $1/B_\nu$, $\nu = 1, 2, ...$), we observe peaks of Ω which indicate the local maxima of potential and the peaks are separated by a period of 0.13 T^{-1}. At $1/B_\nu$, the νth LLs at the K and K' valleys exactly match the chemical potential μ and thus we get

$$\nu = \frac{\mu^2 - (\Delta/2)^2}{2\hbar {v_F}^2 e B_\nu} = \frac{\hbar A_F}{2\pi e B_\nu}, \tag{23}$$

where $A_F = \pi {k_F}^2 = \pi[\mu^2 - (\Delta/2)^2]/(\hbar v_F)^2$ is the area of the Fermi surface of the Dirac system. The rightmost side of Eq. (23) is the relation derived by Onsager [42] to demonstrate that the dHvA oscillation can be utilized to reconstruct the Fermi surface in metals. The period of the dHvA oscillation in the massive Dirac system is given as follows [4,28]:

$$P = \frac{1}{B_\nu} - \frac{1}{B_{\nu-1}} = \frac{2\hbar {v_F}^2 e}{\mu^2 - (\Delta/2)^2}. \tag{24}$$

In the middle and upper panels of Fig. 6(a), we plot Ω by adopting $\mu = 100/\sqrt{2}$ meV ≈ 70.7 meV, $\Delta = 0$ meV and $\mu = 100$ meV, $\Delta = 100\sqrt{2}$ meV ≈ 141.4 meV, respectively. In the both cases, the periods of the oscillation are doubled, which is consistent with Eq. (24). Thus, the period of the dHvA oscillation can be used to extract the value of μ relative to the band gap Δ. This method is originally proposed by Sharapov *et al.* [28] to detect the opening of the band gap in

graphene with keeping μ constant. Experimentally, the band-gap opening was observed [43] in epitaxially grown graphene on the SiC substrate, where $\Delta \approx 0.26$ eV is observed by breaking of sublattice symmetry due to the graphene-substrate interaction.

In Fig. 6(b) we plot magnetizations for the corresponding values of μ and Δ provided in Fig. 6(a), where the oscillations exhibit a sawtoothlike feature. It is known from the LK theory that the sawtoothlike oscillation is a characteristic of the dHvA effect in 2D systems [28,36,37,44,45]. We show that the sawtooth oscillation of M can be explained from the zeta functions in Eqs. (9) and (11). By using the formula $\partial\zeta(p,q)/\partial q = -p\zeta(p+1,q)$, the magnetization is analytically expressed as follows:

$$M = \frac{4e}{h}\left[\frac{3}{2}\hbar\omega_c\zeta\left(-\frac{1}{2},\phi\right) + \mu\left(\nu+\frac{1}{2}\right) - \mu\tilde{\nu}\sum_{\nu}\delta(\tilde{\nu}-\nu) - \frac{1}{2}\hbar\omega_c\zeta\left(\frac{1}{2},\phi\right)\left\{\Gamma^2 + \tilde{\nu}\sum_{\nu}\delta(\tilde{\nu}-\nu)\right\}\right], \tag{25}$$

where we define $\phi \equiv \Gamma^2 + \nu + 1$. Thus, the sawtoothlike oscillation in the magnetization originates from the delta function at $\tilde{\nu} = \nu$ in Eq. (25), which is the result of differentiation of the floor function in the expression of ν [$\partial\lfloor x\rfloor/\partial x = \sum_{n\in\mathbb{Z}}\delta(x-n)$]. Physically, the delta function indicates the occupations of electrons in the discrete LLs. With the increase of temperature, impurity scattering, electron-electron interactions, and electron-phonon interactions [28,46–48], the LLs become broad in which the delta function is replaced by some distribution functions to account for the broadening by the interactions. As a result, the oscillation of magnetization becomes less sharp. The effects of the broadening on the dHvA oscillation can be incorporated by the convolution of the thermodynamic potential at $T = 0$ K with the distribution functions for temperature and impurities, as given in references [28,49,50].

We observe that in the cases of $\Delta = 0$ (doped graphene) [solid and dashed lines in Fig. 6(b)], the smaller μ not only yields a decreasing frequency but also a weaker amplitude in the oscillation. When we consider the cases of $\sqrt{\mu^2 - (\Delta/2)^2} = 70.7$ meV (dashed and dash-dotted lines), the magnetization with the nonzero band gap (dash-dotted line) produces a smaller amplitude in the oscillation than the case with zero band gap (dashed line). The effect of Δ on the amplitude of the oscillation appears in the last term of Eq. (25) [$\Gamma = \Delta/(2\hbar\omega)$], and therefore the opening of band gap decreases the amplitude of the magnetization, as the functions $\zeta(-1/2,\phi)$ and $\zeta(1/2,\phi)$ possess the same signs for a given ϕ (see Appendix B). It is noted that for strong magnetic field ($\hbar\omega_c > \sqrt{\mu^2 - (\Delta/2)^2}$, which gives $\nu = 0$), Eq. (25) will reduce to $M \propto -\sqrt{B}$ because of the linear dependence on ω_c, which will be retained with a small increase of temperature ($\hbar\omega_c \gg k_BT$).

We briefly comment on the possible behavior of the dHvA effect in the case of a fixed electron density N, which originates from the oscillation of chemical potential $\mu(B)$. In this case, the dHvA effect has the same period as that of the oscillation with a fixed μ and only differs in phase because of the existence of the zeroth LLs at the K' valley. The explanation of the statement is given by Appendix C.

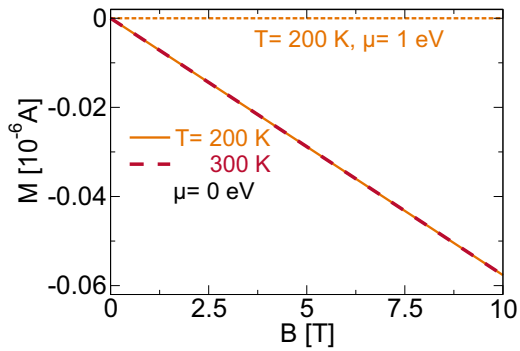

FIG. 7. Magnetization of undoped and doped ($\mu = 1$ eV) MoS_2 as a function $B = 0$–10 T at $T = 200$ and 300 K.

E. Magnetization of TMDs [$(k_BT \sim \hbar\omega_c) \ll \Delta, \lambda \neq 0$, any μ]

For monolayer TMDs in a magnetic field B up to ~10 T, the LLs that are given by Eq. (3) are approximated by $\epsilon_n^\xi \approx \xi\lambda - \Delta/2 - (\hbar\omega_c)^2|n|/\Delta_\xi$ and $\epsilon_n^\xi \approx \Delta/2 + (\hbar\omega_c)^2|n|/\Delta_\xi$ for $\mathrm{sgn}_\tau(n) = -1$ and $\mathrm{sgn}_\tau(n) = +1$, respectively. Thus, the LLs separation is inversely proportional to the band gap, i.e., $(\hbar\omega_c)^2/\Delta_\xi$. This approximation is also valid for heavy Dirac systems such as h-BN where $\Delta \approx 6$ eV [51–53] by putting $\lambda = 0$. The total thermodynamic potential of TMDs is given by (see Appendix A 4 for derivation):

$$\Omega \approx \frac{e^2{v_F}^2B^2}{6\pi}\sum_{\xi=\pm}\frac{1}{\Delta_\xi}\frac{\sinh\left[\frac{\beta\Delta_\xi}{2}\right]}{\cosh\left[\frac{\beta\Delta_\xi}{2}\right] + \cosh\left[\beta\left(\mu - \frac{\xi\lambda}{2}\right)\right]}. \tag{26}$$

From Eq. (26), we can see that $\Omega \propto B^2$ and therefore the magnetization is linearly proportional to B, which prevails only for heavy Dirac fermions.

In Fig. 7, we plot M of undoped MoS_2 as a function of B for $B = 0$–10 T at $T = 200$ K and 300 K, where the magnetization does not change with increasing temperature from $T = 200$ K to 300 K. Thus, even though the magnitude of magnetization in a heavy Dirac fermion decreases with the increasing band gap, the magnetization is robust for temperature. The temperature-independent behavior originates from the energy of the zeroth LLs. In Sec. III C, we have shown that for graphene, the T-dependent is mainly contributed by entropy of the zeroth LLs for $\hbar\omega_c \gg k_BT$ and thermal excitation from valence to conduction bands for $\hbar\omega_c \ll k_BT$. In a heavy Dirac fermion, on the other hand, the energy gap is much larger than the thermal energy $\Delta \gg k_BT$, therefore electrons cannot be thermally excited from the valence to conduction bands. Furthermore, since the zeroth LL at the K valley is fully occupied, the zeroth LL does not contribute to the entropy as in the case of undoped graphene. As a result, magnetization of the heavy Dirac fermion is temperature independent. We also plot M for a doped case ($\mu = 1$ eV) at $T = 200$ K, where the magnetization becomes zero. This phenomenon demonstrates the effect of pseudospin paramagnetism [9,10], as discussed

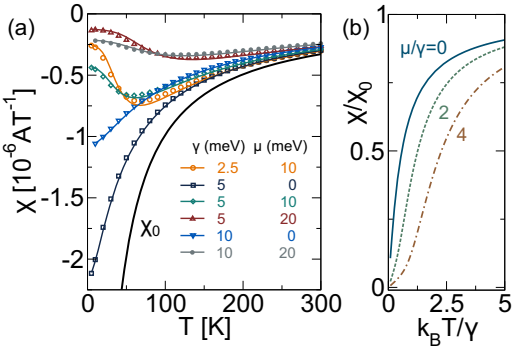

FIG. 8. Susceptibility of graphene with impurity as a function of temperature. (a) The calculations of χ as a function of $T = 0$–300 K for several values of γ and μ with the Faddeeva function (solid lines) and numerical calculations (symbols). (b) The scaled susceptibility χ/χ_0 as a function of k_BT/γ for $\mu/\gamma = 0,\ 2$, and 4 with the Faddeeva function.

by Koshino and Ando [9,10] with the Euler-Maclaurin formula.

F. Susceptibility of graphene and TMDs with impurity

Finally, we analyze the effect of impurity scattering on the orbital susceptibility of the Dirac fermions by using Eq. (8) for susceptibility. In the case of graphene, we approximate the function $\mathrm{sech}^2(\beta\varepsilon/2)$ in Eq. (19) by a Gaussian function $\exp[-(C\beta\varepsilon)^2]$, where C is a constant defined by $C \equiv \sqrt{\ln 2}/[\sqrt{2}\ln(2+\sqrt{3})] \approx 0.447$ (see Appendix D for detail). Therefore Eq. (8) is given by convolution of the Gaussian with the Lorentzian functions, which is known as the Voigt profile. The solution of the Voigt profile is given by the real part of the Faddeeva function $w(z)$ as follows [33]:

$$V(x,y,\sigma) \equiv \frac{y}{\pi}\int_{-\infty}^{\infty} dt \frac{\exp[-t^2/(2\sigma^2)]}{(t-x)^2+y^2} = \mathrm{Re}[w(z)], \quad (27)$$

where σ is the standard deviation of the Gaussian function, $z \equiv (x+iy)/(\sqrt{2}\sigma)$, and $w(z)$ is the Faddeeva function defined by

$$w(z) \equiv e^{-z^2}\left(1 + \frac{2i}{\sqrt{\pi}}\int_0^z dt e^{t^2}\right). \quad (28)$$

Therefore, in the presence impurity, the orbital susceptibility of graphene is approximately given by

$$\chi(\mu,\gamma) \approx -\frac{e^2 {v_F}^2}{6\pi k_B T}\mathrm{Re}[w(z')], \quad (29)$$

where we define $z' \equiv C\beta(\mu + i\gamma)$.

In Fig. 8(a), we plot the susceptibility graphene as a function of temperature for several values of γ and μ by using Eq. (29) (lines) as well as by numerical calculation of the convolution by using the $\mathrm{sech}^2(\beta\varepsilon/2)$ function (symbols). We can see that the approximation with the Faddeeva function is in good agreement with the numerical calculation. For comparison, we show susceptibility of undoped graphene without impurity χ_0 by putting $\mu = 0$ in Eq. (19) [$\chi_0 = -(ev_F)^2/(6\pi k_BT)$], which is inversely proportional to the temperature. From Fig. 8(a), the susceptibility for nonzero

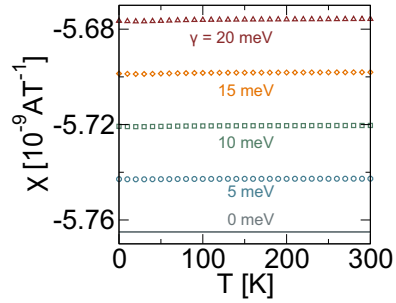

FIG. 9. Susceptibility of undoped MoS_2 with impurity as a function of temperature $T = 0$–300 K for $\gamma = 0,\ 5,\ 10$, and 20 meV.

γ is finite as $T \to 0$ K, which shows that the anomalous diamagnetism in graphene disappears by introducing the impurity effect. In the cases of $\mu \neq 0$, we observe minimum values of χ at finite temperatures. For $\gamma = 5$ meV, the minimum value becomes smaller and shifts to higher temperature as we increase μ from 10 meV to 20 meV. The present method reproduces the calculation by Nakamura and Hirasawa [31], where the susceptibility of graphene with impurity is approximated by the Sommerfeld expansion and also shows the minimum values as a function of temperature. In Fig. 8(b), we plot χ/χ_0 as a function of k_BT/γ. For a given ratio μ/γ, the curves shown in Fig. 8(a) follow the scaling law shown in Fig. 8(b). Therefore, the advantage of using the Faddeeva function is that the susceptibility of graphene in the presence of the impurity scattering is approximately scaled by the function $\mathrm{Re}[w(z')]$.

In Fig. 9, we numerically calculate susceptibility of undoped MoS_2 as a function of T for several values of γ. Here, χ does not change with increasing T. As we increase γ, the magnitude of χ decreases with the same rate, which means that for a given temperature, the magnitude of susceptibility decreases linearly as a function of γ.

IV. CONCLUSION

In this study, the analytical expressions of thermodynamic potentials and magnetizations of the Dirac fermions are derived by using the technique of zeta function regularization. There are four main results obtained in the study: (1) The analytical formula reproduces the Langevin fitting for magnetization of graphene for two limits of $\hbar\omega_c \gg k_BT$ and $\hbar\omega_c \ll k_BT$. (2) We derive the formula for magnetization of heavy Dirac fermions and show that the magnetization is robust with respect to temperature and impurity scattering. (3) The scaling law for orbital susceptibility of graphene with impurity scattering can be approximated by the real part of the Faddeeva function. (4) The gap effect on the dHvA oscillation at $T = 0$ K is discussed from the property of the zeta function in the thermodynamic potential. All results by taking zeta function regularization reproduce the previous works by taking some limits. Thus, the zeta function regularization is justified without any exceptions.

Note added. Recently, we became aware of an experimental work on the detection of divergent orbital diamagnetism of graphene by Vallejo *et al.* [54], where the expression of Ω of

graphene is obtained by using the Fresnel integral, which well agrees with our analytical formulas.

ACKNOWLEDGMENTS

F.R.P. acknowledges MEXT scholarship. M.S.U. and R.S. acknowledge JSPS KAKENHI Grant No. JP18H01810 and CICS, Tohoku University. We thank Dr. E. H. Hasdeo for the useful comments.

APPENDIX A: DERIVATION OF EQS. (9), (11), (13), AND (26)

1. Derivation of Eq. (9)

By substituting $\epsilon_n^\xi = \xi\lambda/2 - \hbar\omega_c\sqrt{|n| + {\Gamma_\xi}^2}$ for $n \leqslant 0$ in the expression of Ω_-, we get

$$\Omega_- = \frac{eB}{h}\sum_{\xi=\pm}\left[\sum_{n=0}^{\infty} + \sum_{n=1}^{\infty}\right]\left[\frac{\xi\lambda}{2} - \hbar\omega_c\sqrt{n + {\Gamma_\xi}^2} - \mu\right], \tag{A1}$$

where the summation operator which begins from $n = 0$ ($n = 1$) operates on the LLs at the K (K') valley. Now, let us shift the index of the summation from $n = 1$ to $n = 0$ for the term $-\hbar\omega_c\sqrt{n + {\Gamma_\xi}^2}$ as follows:

$$\Omega_- = \frac{eB}{h}\sum_{\xi=\pm}\left[\frac{\xi\lambda}{2} + 2\sum_{n=1}^{\infty}\frac{\xi\lambda}{2} - \mu - 2\sum_{n=1}^{\infty}\mu + \frac{\Delta_\xi}{2} - 2\hbar\omega_c\sum_{n=0}^{\infty}\sqrt{n + {\Gamma_\xi}^2}\right]. \tag{A2}$$

The first and the second summations are expressed by the Riemann zeta function $\zeta(p) = \sum_{k=1}^{\infty} 1/k^p$, while the third summation is expressed by the Hurwitz zeta function [Eq. (10)]. By using $\sum_{n=1}^{\infty} = \zeta(0) = -1/2$, we derive the Ω_- as given by Eq. (9).

For heavy fermion ($\Delta_\xi/2 \gg k_BT$), Eq. (A2) can be simplified by using the asymptotic form of $\zeta(p, q)$ for $q \to \infty$ and $p \neq 1$,

$$\zeta(p, q) \sim \frac{q^{1-p}}{p-1} + \frac{q^{-p}}{2} + \frac{1}{12}pq^{-(1+p)}. \tag{A3}$$

Therefore, Ω_- of a heavy Dirac fermion ($\Delta_\xi/2 \gg \hbar\omega_c$) is given by

$$\Omega_- \approx \sum_{\xi=\pm}\left(\frac{1}{24\pi}\frac{{\Delta_\xi}^3}{(\hbar v_F)^2} + \frac{eB}{h}\frac{(\hbar\omega_c)^2}{6\Delta_\xi}\right). \tag{A4}$$

2. Derivation of Eq. (11)

By substituting $\epsilon_n^\xi = \xi\lambda/2 + \hbar\omega_c\sqrt{|n| + {\Gamma_\xi}^2}$ for $n \geqslant 0$, $\Omega_+^{(e)}$ is given by

$$\Omega_+^{(e)} = \frac{eB}{h}\sum_{\xi=\pm}\left[\sum_{n=1}^{\nu_\xi} + \sum_{n=0}^{\nu_\xi}\right]\left[\frac{\xi\lambda}{2} + \hbar\omega_c\sqrt{n + {\Gamma_\xi}^2} - \mu\right] \times \Theta(\mu - \Delta/2)$$

$$= \frac{eB}{h}\sum_{\xi=\pm}\left[\left(\frac{\xi\lambda}{2} - \mu\right)(2\nu_\xi + 1) - \frac{\Delta_\xi}{2} + 2\hbar\omega_c\sum_{n=0}^{\nu_\xi}\sqrt{n + {\Gamma_\xi}^2}\right]\Theta(\mu - \Delta/2). \tag{A5}$$

By expressing the summation of n as the difference of two zeta functions [see Eq. (12)], we get Eq. (11) in the main text.

In the case of hole-doped system, we redefine ν_ξ as the highest unoccupied LLs in the valence bands, and we define $\Omega_-^{(h)}$ as potential from the unoccupied LLs. With the same procedure to derive $\Omega_+^{(e)}$, and by using $\Omega_-^{(h)}$ is given as follows:

$$\Omega_-^{(h)} = \frac{2eB}{h}\sum_{\xi=\pm}\left[\frac{\Delta}{4} + |\mu|\left(\nu_\xi + \frac{1}{2}\right) + \frac{\xi\lambda}{2}\nu_\xi + \hbar\omega_c\left\{\zeta\left(-\frac{1}{2}, {\Gamma_\xi}^2 + \nu_\xi + 1\right) - \zeta\left(-\frac{1}{2}, {\Gamma_\xi}^2\right)\right\}\right] \times \Theta(|\mu| - \Delta_\xi/2). \tag{A6}$$

The total thermodynamic potential is given by $\Omega = \Omega_- - \Omega_-^{(h)}$. It is noted that the electron- and hole-doped Dirac systems give identical Ω for $\lambda = 0$, because of the electron-hole symmetry.

It is noted that we should consider spin magnetization for the hole doping when chemical potential is located between $n = 0$ LLs for up and down spins, i.e., $-\Delta/2 - \lambda < \mu < -\Delta/2 + \lambda$. For example, in the case of Figs. 1(e) and 1(f), -0.905 eV $< \mu < -0.755$ eV. Here, the number of the down spin electron is larger than that of the up spin because of the occupancy of down spin at $n = 0$ LL at the K valley. The difference of the numbers of down and up spins electrons is one per degeneracy of the LL (eB/h). It means that the magnitude of induced spin magnetization is given by $|M_{\rm spin}| = (eB/h)\mu_B$, where $\mu_B = 9.274 \times 10^{-24}$ J/T is the Bohr magneton. Therefore, $M_{\rm spin}$ is proportional to B, which is similar to the conventional Zeeman effect. Nevertheless, the proportionality of B in the Zeeman effect comes from the energy splitting $g\mu_B B$ ($g \approx 2$ is the g factor). The calculated value of $|M_{\rm spin}|$ for $B = 1$ T is 2.24×10^{-9} A, which is comparable to the orbital magnetization in MoS_2, $M \approx -6 \times 10^{-9}$ A (see Fig. 7). For such hole doping, the slope of total magnetization as a function of B is modified from the orbital magnetization.

3. Derivation of Eq. (13)

The thermodynamic potential Ω'_+ for $T > 0$ K is calculated by convolution of $\Omega'_{+0} \equiv \Omega'_+(T = 0\,\text{K})$ with $(-\partial f/\partial\varepsilon) = \beta\,\text{sech}^2[\beta(\varepsilon - \mu)/2]/4$, where $f(\varepsilon)$ is the Fermi distribution function [4,28]. By using $\epsilon_n = \hbar\omega_c\sqrt{|n| + \Gamma^2}$, Ω'_{+0} is given by

$$\Omega'_{+0} = 2g_s\frac{eB}{h}\sum_{n=\nu+1}^{\infty}[\epsilon_n - \mu] = 2g_s\frac{eB}{h}\left[\hbar\omega_c\zeta\left(-\frac{1}{2}, \Gamma^2 + \nu + 1\right) + \left(\nu + \frac{1}{2}\right)\mu\right]. \tag{A7}$$

Here, in the second line of Eq. (A7) we use $\sum_{n=\nu+1}^{\infty} = \zeta(0) - \sum_{n=1}^{\nu} = -(1/2+\nu)$. Let us consider $\mu \gg \hbar\omega_c$. Because in this case $\Gamma^2+\nu+1 \approx \mu^2/(\hbar\omega_c)^2$, the zeta function $\zeta(-1/2, \Gamma^2+\nu+1)$ can be approximated by using Eq. (A3). Ω'_{+0} and Ω'_{+} are given by

$$\Omega'_{+0}(\mu) \approx \frac{1}{2\pi}\frac{g_s}{(\hbar v_F)^2}\left[\frac{\mu^3}{3} - \frac{\Delta^2\mu}{4} - \frac{(\hbar\omega_c)^4}{24\mu}\right] \tag{A8}$$

and

$$\Omega'_{+}(\mu) = \frac{\beta}{4}\int_{-\infty}^{\infty} d\varepsilon\, \Omega'_{+0}(\varepsilon)\,\mathrm{sech}^2\Big[\frac{\beta}{2}(\varepsilon-\mu)\Big], \tag{A9}$$

respectively, where $\Omega'_{+0}(\varepsilon)$ is given by substituting μ in Eq. (A8) to the variable ε. $\Omega'_{+0}(\varepsilon)$ is an odd function of ε. In the case of $\mu \ll k_BT$, the function $\mathrm{sech}^2[\beta(\varepsilon-\mu)/2]$ can be approximated as an even function. Therefore, we get $\Omega'_{+}(\mu) \approx 0$ in the case of $\hbar\omega_c \ll \mu \ll k_BT$.

Now, by expanding the logarithmic and exponential functions in the expression of thermodynamic potential for $\hbar\omega_c \sim \Delta \ll k_BT$ and by using $\epsilon_{-n} = -\hbar\omega_c\sqrt{|n|+\Gamma^2}$, Ω_- is given by

$$\begin{aligned}
\Omega_- &= \frac{-g_s}{\beta}\frac{eB}{h}\left[\sum_{n=0}^{\infty}+\sum_{n=1}^{\infty}\right]\sum_{k=1}^{\infty}\frac{(-1)^{k-1}}{k}e^{\beta\mu k}\exp(-\beta\epsilon_{-n}k)\\
&= \frac{g_s}{\beta}\frac{eB}{h}\left[\sum_{n=0}^{\infty}+\sum_{n=1}^{\infty}\right]\sum_{k=1}^{\infty}\frac{(-e^{\beta\mu})^k}{k}\sum_{l=0}^{\infty}\frac{(-\beta\epsilon_{-n}k)^l}{l!}\\
&= \frac{g_s}{\beta}\frac{eB}{h}\sum_{l=0}^{\infty}\sum_{k=1}^{\infty}\frac{(-e^{\beta\mu})^k}{k^{1-l}}\frac{(\beta\hbar\omega_c)^l}{l!}\\
&\quad\times\left[2\sum_{n=0}^{\infty}(n+\Gamma^2)^{l/2}-\Gamma^l\right]\\
&= \frac{2g_seB}{\beta h}\sum_{l=0}^{\infty}\mathrm{Li}_{1-l}(-e^{\beta\mu})\frac{(\beta\hbar\omega_c)^l}{l!}\left[\zeta\Big(\frac{-l}{2},\Gamma^2\Big)-\frac{\Gamma^l}{2}\right].
\end{aligned} \tag{A10}$$

In the third line of Eq. (A10), we switch the order of summations with indices k and l in order to express the μ dependence of Ω_- in terms of the polylogarithm function $\sum_{k=1}^{\infty}(-e^{\beta\mu})^k/k^{1-l} = \mathrm{Li}_{1-l}(-e^{\beta\mu})$, and we shift the sum operator which begins from $n=1$ to $n=0$ in order to adopt the Hurwitz zeta function. Similarly, the expression for Ω_+ is given by

$$\Omega_+ = \frac{2g_seB}{\beta h}\sum_{l=0}^{\infty}\mathrm{Li}_{1-l}(-e^{\beta\mu})\frac{(-\beta\hbar\omega_c)^l}{l!}\left[\zeta\Big(\frac{-l}{2},\Gamma^2\Big)-\frac{\Gamma^l}{2}\right]. \tag{A11}$$

When we add Eqs. (A10) and (A11), the terms for odd l disappear, while the terms for $l = 0,\ 2,\ 4,\ \ldots$ are doubled. By expressing $l = 2\ell$, we get Eq. (13). By using $\zeta(0,x) = 1/2 - x$ and $\mathrm{Li}_1(z) = -\ln(1-z)$ [33], Ω_0 in Eq. (13) is given by

$$\Omega_0 = k_BT\frac{g_s}{4\pi}\frac{\Delta^2}{(\hbar v_F)^2}\ln[1+e^{\beta\mu}]. \tag{A12}$$

Ω_0 is proportional to the square of band-gap Δ^2 as well as temperature T and does not depend on the magnetic field. As for $\ell = 1$, by using $\mathrm{Li}_{-1}(z) = z/(1-z)^2$, $\zeta(-1,x) = -(1/2)(x^2-x+1/6)$, Ω_1 is given by

$$\Omega_1 = \frac{g_s}{\pi k_BT}\mathrm{sech}^2\Big(\frac{\mu}{2k_BT}\Big)\left[\frac{\Delta^4}{256(\hbar v_F)^2}+\frac{(v_FeB)^2}{24}\right]. \tag{A13}$$

Thus, because of the factor B^2 in the second term Eq. (A13), $M \propto -B/T$. The terms which consist of Δ in the expressions of Ω_0 and Ω_1 can be interpreted as a fraction of energy required to excite electrons from the valence to conduction bands across the band gap.

4. Derivation of Eq. (26)

In the derivation of Eq. (26), we consider $\Omega = \Omega_- + \Omega_+$, because of the small separation of the LLs $[(\hbar\omega_c)^2/\Delta_\xi]$ and therefore thermal excitation can induce indefinite occupation of the LLs at the conduction bands. Ω_- for TMDs is given as follows:

$$\Omega_- = -\frac{1}{\beta}\frac{eB}{h}\sum_{\xi=\pm}\left[\sum_{n=0}^{\infty}+\sum_{n=1}^{\infty}\right]\ln\Big[1+\exp\big\{-\beta\big(\epsilon^{\xi}_{-n}-\mu\big)\big\}\Big]. \tag{A14}$$

By using $\epsilon^{\xi}_{-n} = \xi\lambda - \Delta/2 - (\hbar\omega_c)^2|n|/\Delta_\xi$, we have

$$\begin{aligned}
\Omega_- &= -\frac{1}{\beta}\frac{eB}{h}\sum_{\xi=\pm}\ln[1+e^{\beta(\mu-\xi\lambda+\Delta/2)}]\\
&\quad-\frac{2}{\beta}\frac{eB}{h}\sum_{\xi=\pm}\sum_{n=1}^{\infty}\ln[1+e^{\beta\{\mu-\xi\lambda+\Delta/2+(\hbar\omega_c)^2n/\Delta_\xi\}}]\\
&\equiv \Omega'_- + \Omega''_-.
\end{aligned} \tag{A15}$$

Here, we define Ω'_- and Ω''_- as thermodynamic potentials for the zeroth LL at the K valley and $n \leqslant -1$ LLs, respectively. By expanding the logarithmic and exponential functions in the expression of Ω''_-, we get

$$\begin{aligned}
\Omega''_- &= \frac{2}{\beta}\frac{eB}{h}\sum_{\xi=\pm}\sum_{k=1}^{\infty}\frac{[-e^{(\mu-\xi\lambda+\Delta/2)}]^k}{k}\\
&\quad\times\sum_{l=0}^{\infty}\Big(\frac{\beta k}{\Delta_\xi}\Big)^l\frac{(\hbar\omega_c)^{2l}}{l!}\sum_{n=1}^{\infty}n^l\\
&= \frac{2}{\beta}\frac{eB}{h}\sum_{\xi=\pm}\sum_{l=0}^{\infty}\mathrm{Li}_{1-l}[-e^{\beta(\mu-\xi\lambda+\Delta/2)}]\Big(\frac{\beta}{\Delta_\xi}\Big)^l\\
&\quad\times\frac{(\hbar\omega_c)^{2l}}{l!}\zeta(-l)\\
&= \sum_{l=0}^{\infty}\Omega''_l.
\end{aligned} \tag{A16}$$

Because $\mathrm{Li}_1(z) = -\ln(1-z)$ and $\zeta(0) = -1/2$, we get $\Omega''_0 = eB/(\beta h)\sum_{\xi=\pm1}\ln[1+e^{(\mu-\xi\lambda+\Delta/2)}] = -\Omega'_-$. As a result, only the terms for $l \geqslant 1$ survive in the final expression

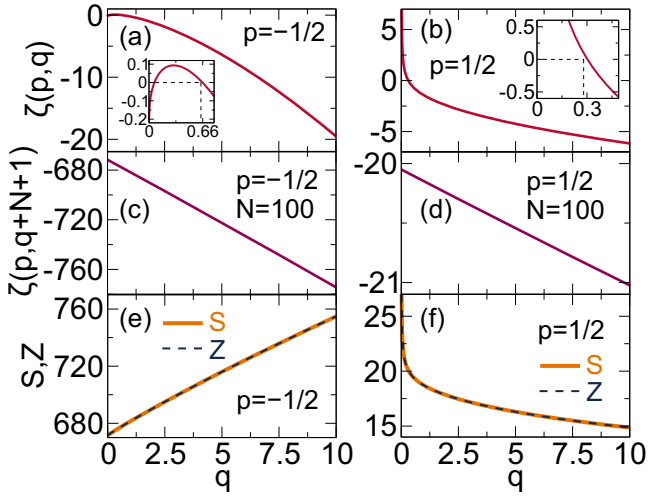

FIG. 10. Plot of $\zeta(p,q)$ with $q = 1$–10 for (a) $p = -1/2$, (b) $p = 1/2$. In the insets of (a) and (b) we show that the values of $\zeta(p,q)$ for $p = -1/2$ and $p = 1/2$ are negative for $q > 0.66$ and $q > 0.3$, respectively. Plot of $\zeta(p, q+N+1)$ with $N = 100$ for (c) $p = -1/2$, (d) $p = 1/2$. The comparison between the functions $S(p,q,N)$ and $Z(p,q,N)$ for (e) $p = -1/2$ and (f) $p = 1/2$.

of Ω_- as follows:

$$\Omega_- = -\frac{2}{\beta}\frac{eB}{h}\sum_{\xi=\pm1}\sum_{l=1}^{\infty}\mathrm{Li}_{1-l}[-e^{\beta(\mu-\xi\lambda+\Delta/2)}]\left(\frac{\beta}{\Delta_\xi}\right)^l \times \frac{(\hbar\omega_c)^{2l}}{l!}\frac{\mathcal{B}_{l+1}}{l+1}. \tag{A17}$$

Therefore, the entropy of electrons at the zeroth LLs is not manifested in a linear T dependence as in the case of graphene, as explained in the main text. In fact, by comparing Eq. (A17) [here, $\mathrm{Li}_0(z) = z/(1-z)$] with (A4), we infer that the magnetizations of the undoped, heavy Dirac fermions at $T = 0$ K and finite temperatures are almost equal, provided that $\Delta_\xi/2 \gg k_B T$. Similarly, by using $\epsilon_n^\xi = \Delta/2 + (\hbar\omega_c)^2|n|/\Delta_\xi$ for $n \geqslant 0$, we can derive Ω_+ of TMDs as follows:

$$\Omega_+ = -\frac{2}{\beta}\frac{eB}{h}\sum_{\xi=\pm1}\sum_{l=1}^{\infty}\mathrm{Li}_{1-l}[-e^{\beta(\mu-\Delta/2)}]\left(\frac{-\beta}{\Delta_\xi}\right)^l \times \frac{(\hbar\omega_c)^{2l}}{l!}\frac{\mathcal{B}_{l+1}}{l+1}. \tag{A18}$$

APPENDIX B: NUMERICAL CALCULATIONS OF THE ZETA FUNCTION

In Figs. 10(a) and 10(b), we plot the zeta function $\zeta(p,q)$ for $p = -1/2$ and $p = 1/2$, respectively. The value of $\zeta(-1/2,q)$ is negative and deceases monotonically for $q > 0.66$ as shown in the inset in (a). The value of $\zeta(1/2,q)$ diverges at $q = 0$ and change signs at $q \approx 0.3$. In (c) and (d), we substitute q to $q+N+1$ and take $N = 100$ for explaining the change of $\zeta(p,q) - \zeta(p,q+N+1)$. In (e) and (f) we compare the functions $S(p,q,N) \equiv \sum_{n=0}^{N}(n+q)^{-p}$ and $Z(p,q,N) \equiv \zeta(p,q) - \zeta(p,q,N+1)$, similar to the left-hand and right-hand sides of Eq. (12), respectively. It is observed that the two functions are exactly identical for $q = 0$ to 10.

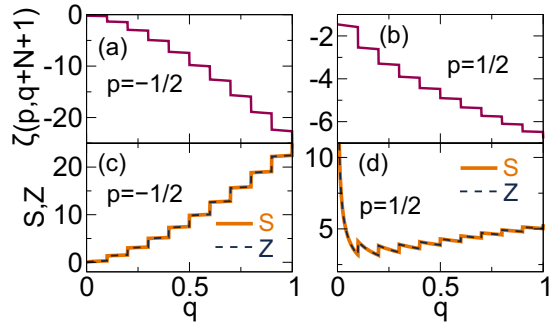

FIG. 11. Plot of $\zeta(p, q+N+1)$ with $N = 10\lfloor q \rfloor$ for (a) $p = -1/2$, (b) $p = 1/2$. The comparison between the functions $S(p,q,N)$ and $Z(p,q,N)$ for (c) $p = -1/2$ and (d) $p = 1/2$.

It is noted that both the functions S and Z are continuous and do not explain the oscillatory behavior of the thermodynamic potential in the dHvA effect. By changing the constant N to $10\lfloor q \rfloor$ for an example, the function $\zeta(p, q+N+1)$ shows steplike behavior as shown in Figs. 11(a) and 11(b) because of the nature of the function $\lfloor q \rfloor$. In (c) and (d), we compare the functions $S(p,q,N)$ and $Z(p,q,N)$ for $p = -1/2$ and $p = 1/2$, respectively. As in the previous case, the two functions match each other. Therefore, the analytical expressions of the thermodynamic potentials for doped Dirac fermion is numerically verified.

APPENDIX C: dHvA EFFECT FOR CONSTANT ELECTRON DENSITY N

We discuss the possible behavior of the dHvA effect in the case of fixed electron density N [$1/\mathrm{m}^2$]. Here, the dHvA effect is originated from the oscillation of $\mu(B)$, which will be derived as follows. N is given by the spin and LL degeneracies multiplied by the number of occupied LLs at the conduction bands, as follows:

$$N = g_s\frac{eB}{h}(2\nu+1), \tag{C1}$$

where the factor 2 for 2ν comes from the valley degeneracy, and the term 1 inside the bracket represents the zeroth LL at the K' valley. From Eq. (C1), ν for a fixed N is given by

$$\nu = \left\lfloor \frac{1}{2}\left(\frac{Nh}{g_s eB} - 1\right)\right\rfloor. \tag{C2}$$

In Eq. (C2), the density of electron N can also be obtained from the Fermi energy at zero magnetic field $\epsilon_F = \sqrt{(\hbar v_F k_F)^2 + (\Delta/2)^2}$, that is,

$$N = 2g_s\frac{\pi {k_F}^2}{(2\pi)^2} = \frac{g_s}{2\pi}\frac{{\epsilon_F}^2 - \Delta^2/4}{(\hbar v_F)^2}. \tag{C3}$$

For a given B, the chemical potential is equal to the highest LL $\epsilon_\nu(B)$, and thus $\mu(B) = \epsilon_\nu(B) = \sqrt{2\hbar {v_F}^2 eB\nu + \Delta^2/4}$.

In Fig. 12(a), we plot $\mu(B)$ (red-dashed line) for $\epsilon_F = 100$ meV, superimposed on the $n = 0$–7 LLs (gray-solid lines). We can see that $\mu(B)$ falls to the lower LLs one by

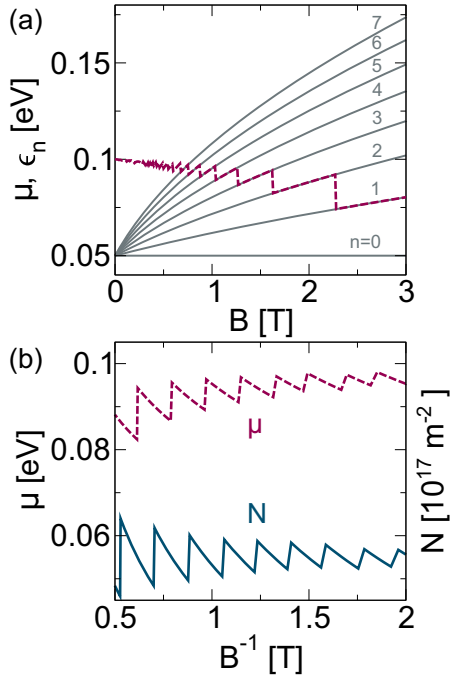

FIG. 12. Oscillations of (a) $\mu(B)$ superimposed on the $n = 0$–7 LLs at the K' valley and (b) $\mu(B)$ and $N(B)$ as a function of B^{-1}. In (a) and (b), we take $\epsilon_F = 100$ meV and $T = 0$ K.

one by increasing B. It is noted that we need to take special care for the occupancy in the $n = 0$ LL for a large magnetic field since there is only one zeroth LL at the conduction bands, which we do not discuss here. At B_ν, μ undergoes transition from ϵ_ν to $\epsilon_{\nu-1}$, and the corresponding ν is as follows:

$$\nu = \frac{{\epsilon_F}^2 - \Delta^2/4}{2\hbar {v_F}^2 e B_\nu} - \frac{1}{2}. \tag{C4}$$

From Eq. (C4), the period of oscillation is given by

$$P = \frac{2\hbar {v_F}^2 e}{{\epsilon_F}^2 - \Delta^2/4}, \tag{C5}$$

which is identical to Eq. (24). In Fig. 12(b), we compare the oscillations for $\mu(B)$, with keeping N constant (red-dashed line) and $N(B)$, with keeping μ constant (blue-solid line). In the case of keeping μ constant, $N(B)$ is given by

$$N(B) = g_s \frac{eB}{h}\left(2\left\lfloor \frac{\mu^2 - \Delta^2/4}{2\hbar {v_F}^2 eB} \right\rfloor + 1\right). \tag{C6}$$

It is observed that $\mu(B)$ oscillates with different a phase to that of $N(B)$.

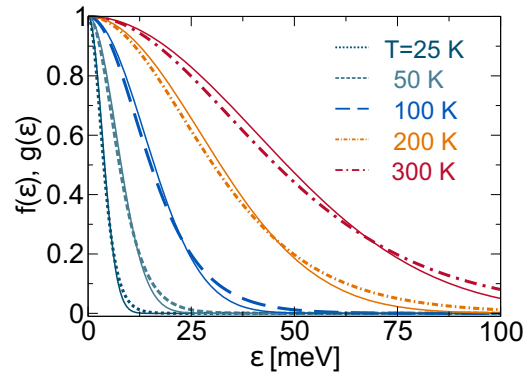

FIG. 13. Comparison between the functions $f(\varepsilon)$ and $g(\varepsilon)$ (thin-solid lines) for $T = 25,\ 50,\ 100,\ 200$, and 300 K.

APPENDIX D: APPROXIMATION OF $\mathrm{sech}^2(\beta\epsilon/2)$ TO A GAUSSIAN FUNCTION

For given secant-hyperbolic and the Gaussian distributions, $F(\varepsilon) \equiv \mathrm{sech}(\varepsilon/W)$ and $G(\varepsilon) \equiv \exp[-\varepsilon^2/(2\sigma^2)]$, respectively, the half width of the distributions are given by $\mathrm{HW}_F = \ln(2+\sqrt{3})W$ and $\mathrm{HW}_G = \sqrt{2\ln(2)}\sigma$. By solving $\mathrm{HW}_F = \mathrm{HW}_G$ and choosing $W = 2/\beta$, the Gaussian approximation for the function $f(\varepsilon) \equiv \mathrm{sech}^2(\beta\varepsilon/2)$ is given by $g(\varepsilon) \equiv \exp[-(C\beta\varepsilon)^2]$, where $C = \sqrt{\ln 2}/[\sqrt{2}\ln(2+\sqrt{3})] \approx 0.447$ as defined in the main text. In Fig. 13, we compare $f(\varepsilon)$ and $g(\varepsilon)$ (thin-solid lines) for several values of temperature. The distribution $g(\varepsilon)$ has a smaller tail compared with $f(\varepsilon)$, which is the origin of discrepancies between the numerical calculation and the Faddeeva approximation for $\chi(\mu, \gamma)$.

[1] M. Sepioni, R. R. Nair, S. Rablen, J. Narayanan, F. Tuna, R. Winpenny, A. K. Geim, and I. V. Grigorieva, Phys. Rev. Lett. **105**, 207205 (2010).
[2] M. O. Goerbig, Rev. Mod. Phys. **83**, 1193 (2011).
[3] Y. Fuseya, M. Ogato, and H. Fukuyama, J. Phys. Soc. Jpn. **84**, 012001 (2015).
[4] J. W. McClure, Phys. Rev. **104**, 666 (1956).
[5] R. Saito and H. Kamimura, Phys. Rev. B **33**, 7218 (1986).
[6] A. Raoux, M. Morigi, J.-N. Fuchs, F. Piéchon, and G. Montambaux, Phys. Rev. Lett. **112**, 026402 (2014).
[7] A. Principi, M. Polini, G. Vignale, and M. I. Katsnelson, Phys. Rev. Lett. **104**, 225503 (2010).
[8] A. Principi, M. Polini, and G. Vignale, Phys. Rev. B **80**, 075418 (2009).
[9] M. Koshino and T. Ando, Phys. Rev. B **81**, 195431 (2010).
[10] M. Koshino and T. Ando, Solid State Commun. **151**, 1054 (2011).
[11] H. Fukuyama, Y. Fuseya, M. Ogato, A. Kobayashi, and Y. Suzumura, Physica B **407**, 1943 (2012).
[12] L. Landau, Z. Phys. **64**, 629 (1930).
[13] T. Cai, S. A. Yang, X. Li, F. Zhang, J. Shi, W. Yao, and Q. Niu, Phys. Rev. B **88**, 115140 (2013).
[14] M. Koshino and I. F. Hizbullah, Phys. Rev. B **93**, 045201 (2016).
[15] B. Van Duppen and F. M. Peeters, Phys. Rev. B **88**, 245429 (2013).
[16] X.-Z. Yan and C. S. Ting, Phys. Rev. B **96**, 104403 (2017).
[17] Z. Li, L. Chen, S. Meng, L. Guo, J. Huang, Y. Liu, W. Wang, and X. Chen, Phys. Rev. B **91**, 094429 (2015).

[18] D. Cangemi and G. Dunne, Ann. Phys. (NY) **249**, 582 (1996).
[19] A. Ghosal, P. Goswami, and S. Chakravarty, Phys. Rev. B **75**, 115123 (2007).
[20] S. Slizovskiy and J. J. Betouras, Phys. Rev. B **86**, 125440 (2012).
[21] G.-B. Liu, W.-Y. Shan, Y. Yao, W. Yao, and D. Xiao, Phys. Rev. B **88**, 085433 (2013).
[22] W.-K. Tse and A. H. MacDonald, Phys. Rev. B **84**, 205327 (2011).
[23] J. L. Lado and J. Fernández-Rossier, 2D Mater. **3**, 035023 (2016).
[24] C. J. Tabert and E. J. Nicol, Phys. Rev. Lett. **110**, 197402 (2013).
[25] F. Qu, A. C. Dias, J. Fu, L. Villegas-Lelovsky, and D. L. Azevedo, Sci. Rep. **7**, 41044 (2017).
[26] X. Li, F. Zhang, and Q. Niu, Phys. Rev. Lett. **110**, 066803 (2013).
[27] D. Xiao, G.-B. Liu, W. Feng, X. Xu, and W. Yao, Phys. Rev. Lett. **108**, 196802 (2012).
[28] S. G. Sharapov, V. P. Gusynin, and H. Beck, Phys. Rev. B **69**, 075104 (2004).
[29] M. Koshino and T. Ando, Phys. Rev. B **75**, 235333 (2007).
[30] M. Nakamura, Phys. Rev. B **76**, 113301 (2007).
[31] M. Nakamura and L. Hirasawa, Phys. Rev. B **77**, 045429 (2008).
[32] C. J. Tabert, J. P. Carbotte, and E. J. Nicol, Phys. Rev. B **91**, 035423 (2015).
[33] F. W. J. Olver, D. W. Lozier, R. F. Boisvert, and C. W. Clark (eds.), *NIST Handbook of Mathematical Functions* (Cambridge University Press, New York, 2010).
[34] M. Ezawa, Eur. Phys. J. B **85**, 363 (2012).
[35] I. A. Luk'yanchuk and Y. Kopelevich, Phys. Rev. Lett. **93**, 166402 (2004).
[36] T. Champel and V. P. Mineev, Philos. Mag. B **81**, 55 (2001).
[37] K. Kishigi and Y. Hasegawa, Phys. Rev. B **65**, 205405 (2002).
[38] I. A. Luk'yanchuk, Low Temp. Phys. **37**, 45 (2011).
[39] A. R. Wright and R. H. McKenzie, Phys. Rev. B **87**, 085411 (2013).
[40] K. Kishigi and Y. Hasegawa, Phys. Rev. B **90**, 085427 (2014).
[41] I. M. Lifshitz and A. M. Kosevich, Sov. Phys. JETP **2**, 636 (1956).
[42] L. Onsager, Philos. Mag. **43**, 1006 (1952).
[43] S. Y. Zhou, G.-H. Gweon, A. V. Fedorov, P. N. First, W. A. de Heer, D.-H. Lee, F. Guinea, A. H. Castro Neto, and A. Lanzara, Nat. Mater. **6**, 770 (2007).
[44] F. Escudero, J. S. Ardenghi, and P. Jasen, J. Phys.: Condens. Matter **31**, 285804 (2019).
[45] F. Escudero, J. S. Ardenghi, and P. Jasen, Eur. Phys. J. B **93**, 93 (2020).
[46] C. H. Yang, F. M. Peeters, and W. Xu, Phys. Rev. B **82**, 075401 (2010).
[47] H. Funk, A. Knorr, F. Wendler, and E. Malic, Phys. Rev. B **92**, 205428 (2015).
[48] O. O. Sobol, P. K. Pyatkovskiy, E. V. Gorbar, and V. P. Gusynin, Phys. Rev. B **94**, 115409 (2016).
[49] J. Knolle and N. R. Cooper, Phys. Rev. Lett. **115**, 146401 (2015).
[50] S. Becker and M. Zworski, Commun. Math. Phys. **367**, 941 (2019).
[51] Y. Kubota, K. Watanabe, O. Tsuda, and T. Taniguchi, Science **317**, 932 (2007).
[52] K. K. Kim, A. Hsu, X. Jia, S. M. Kim, Y. Shi, M. Hofmann, D. Nezich, J. F. Rodriguez-Nieva, M. Dresselhaus, T. Palacios, and J. Kong, Nano Lett. **12**, 161 (2011).
[53] G. Cassabois, P. Valvin, and B. Gil, Nat. Photonics **10**, 262 (2016).
[54] J. Vallejo, N. J. Wu, C. Fermon, M. Pannetier-Lecoeur, T. Wakamura, K. Watanabe, T. Tanigushi, T. Pellegrin, A. Bernard, S. Daddinounou, V. Bouchiat, S. Guéron, M. Ferrier, G. Montambaux, and H. Bouchiat, arXiv:2012.05357.